Unconventional superfluidity of fermions in Bose-Fermi mixtures

O. Dutta[1] and M. Lewenstein[1,2]

[1]*ICFO-Institut de Ciències Fotòniques, Mediterranean Technology Park, E-08860 Castelldefels, Barcelona, Spain*

[2]*ICREA-Instituciò Catalana de Recerca i Estudis Avançats, Lluis Companys 23, E-08010 Barcelona, Spain*

(Received 29 June 2009; revised manuscript received 27 October 2009; published 7 June 2010)

We examine a two-dimensional mixture of single-component fermions and dipolar bosons. We calculate the self-enregies of the fermions in the normal state and the Cooper-pair channel by including first-order vertex correction to derive a modified Eliashberg equation. We predict the appearance of superfluids with various nonstandard pairing symmetries at experimentally feasible transition temperatures within the strong-coupling limit of the Eliashberg equation. Excitations in these superfluids are anyonic and follow non-Abelian statistics.

DOI: 10.1103/PhysRevA.81.063608 PACS number(s): 67.85.Pq, 03.75.−b, 67.85.Jk, 74.20.Rp

I. INTRODUCTION

Experimental realization of fermionic superfluidity in a quantum degenerate ultracold gas [1] started a renewed interest in the field. Attraction between fermionic particles favors the pairing of fermions, resulting in superfluidity of the system. The paired fermions, known as Cooper pairs, can have different kinds of internal symmetries. The common ones found in nature have s-wave and d-wave internal structure and conserve parity and time-reversal symmetry. In superfluid ^{3}He, the so-called A and A_1 phases are characterized by Cooper pairs with nonzero magnetic orbital momenta. Also, there was a theoretical prediction of higher-order f-wave pairing in ^{3}He [2,3]. Classical heavy-fermion noncentrosymmetric compounds with like UPt_3 also show unconventional order parameter with nonzero angular momentum [4]. Cooper pairs with chiral $(p_x + ip_y)$-wave internal structure are believed to be responsible for the observed superfluidity of electrons in strontium ruthenate [5]. This kind of pairing breaks the time-reversal symmetry. The spinless chiral p-wave superfluid state has formal resemblance to the "Pfaffian" state proposed in relation to the fractional quantum Hall state with filling factor 5/2 [6–8]. When confined in a two-dimensional geometry, excitations in the chiral p-wave superfluid become so-called non-Abelian anyons. Anyons are particles living in a two-dimensional plane that, under exchange, behave neither as bosons nor as fermions. For non-Abelian anyons, the exchange of two such particles depends on the order of the exchange [9–11]. Apart from a fundamental interest in the existence of such particles, non-Abelian anyons find remarkable applications in the field of quantum information for quantum memories and fault-tolerant quantum computation [12]. Finally, admixture of order parameters with nonzero angular momentum is considered in Refs. [13,14].

Recently, it has been shown that quasiparticles in vortex excitations of chiral two-dimensional p-wave spinless superfluids obey non-Abelian statistics [15,16]. Using p-wave Feshbach resonances in fermionic ultracold atoms, such superfluids can be realized in principle, but this procedure is very difficult because of nonelastic loss processes [17]. Another proposal for p-wave superfluid with dipolar fermions has been recently formulated in Ref. [18] with transition temperature on the order of $0.1\epsilon_F$, where ϵ_F is the Fermi energy. Bose-Fermi mixtures are another candidate for creating superfluidity in fermions via boson-mediated interactions [19] and have formal resemblance to phonon-mediated superconductivity in metals. It was found, however, when the bosons and single-component fermions are completely mixed, increasing the boson-fermion interaction strength or fermionic density may induce dynamical instability of the condensate, resulting in phase separation in the mixture [19–22]. Near phase separation, inclusion of the dressing of phonons is predicted to increase the transition temperature [23]. In Ref. [24], the authors found that close to Feshbach resonances, a Bose-Einstein condensate of dimers can induce a strong pairing in the p-wave channel. In Refs. [25–29], the authors discuss the stability of p-wave pairing in a repulsive Fermi gas and concentrated Bose-Fermi mixtures within the framework of the Kohn-Luttinger mechanism by including vertex correction and retardation effect and their effect on superconducting transition temperature. In the concentrated He^3-He^4 mixtures the inclusion of vertex-corrections in the framework of the Kohn-Luttinger mechanism as well as the retardation effect stabilizes p-wave pairing in three and two dimensions.

In the present article, we discuss another way to generate high-temperature superfluids in a Bose-Fermi mixture. We study the property of superfluidity in Bose-Fermi mixtures, where bosons are interacting via long-range dipolar interactions. We show that the transition temperature for p-wave superfluidity can become comparable to the Fermi energy. More importantly, we find that other more exotic Cooper pairs with f- and h-wave internal symmetries are possible in a certain range of Fermi energies without bosons and fermions separating. In addition, we study the excitations in chiral states of the odd-wave superfluids and point out their non-Abelian anyonic nature. Experimentally, an available bosonic species, where prominent dipolar interaction can be achieved using Feshbach resonance, is Cr^{52} [30,31]. Another route toward achieving ultracold dipolar gas is to experimentally realize quantum degenerate heteronuclear molecules [32], which have permanent electric moment. Thus, in the near future a quantum degenerate mixture of dipolar bosons and fermions will be achievable experimentally.

In Sec. II we review the properties of a dipolar Bose-Einstein condensate in a pancake trap. We discuss especially the excitation spectrum of such condensates. Then in Sec. III we study the boson-fermion interaction and the many-body effect of fermions on dressing the excitation spectrum of the condensate. In Sec. IV, we discuss the interaction between the fermions mediated by bosons in different angular momentum channels. By integrating out the bosonic mode, we show that the absolute value of the interaction between fermions in the (p,h,f)-wave angular momentum channel are comparable depending on the Fermi energy. In Sec. V, we go beyond Migdal's limit and include first-order vertex corrections to study fermion self-energy in normal state, as well as the mass renormalization function in the high temperature limit. In doing so, we include the full effect of retardation and strong momentum dependence of the bosonic excitation spectrum and bosonic propagator. We find that vertex correction reduces the mass renormalization function. In Sec. VI we calculate the self-energy in a Cooper-pair channel for (p,f,h)-wave order parameters including the vertex correction and cross interaction for temperature $T > T_c$. By deriving a vertex-corrected strong-coupling Eliashberg equation, we solve for transition temperatures in different angular momentum channels. In Sec. VII, we present a brief discussion regarding the possible occurrence of non-Abelian Majorana fermions for broken time-reversal p-, f-, and h-wave superfluids. We solve the Bugoliubov–de Gennes equation for the p-, f-, and h-wave superfluids in the limit of large distance to find the Majorana bound states.

II. DIPOLAR BOSE-EINSTEIN CONDENSATE

Our system consists of dipolar bosons mixed with single-component fermions, confined in a quasi-two-dimensional geometry by a harmonic potential in the z direction with the condition $m_b\omega_b^2 = m_f\omega_f^2$, where m_b and m_f are the mass of bosons and fermions, respectively, and ω_b, ω_f is the trapping frequency. First, we assume that the bosons are polarized along the z direction. The dipolar interaction reads $V_{\rm dd} = \frac{4\pi g_{\rm dd}}{3}(3k_z^2/k^2 - 1)$ in momentum space, where $g_{\rm dd}$ is the dipole-dipole interaction strength. For atoms $g_{\rm dd} = \mu_0\mu_m^2/4\pi$, and for dipolar molecules $g_{\rm dd} = \mu_e^2/4\pi\epsilon_0$, where μ_m and μ_e are the magnetic moment of the atoms and the electric dipole moment of the molecules, respectively. We assume that the z dependence of bosonic density is given by a Thomas-Fermi profile,

$$n_b(x,y,z) = \frac{3n_b}{4R_z}\left(1 - \frac{z^2}{R_z^2}\right),$$

where the Thomas-Fermi radius R_z is determined variationally. After integrating over z dependence of the density profile of bosons, the total interaction takes the form $V_{\rm eff} = \frac{8\pi g_{\rm dd}}{5R_z}\mathcal{V}(\tilde{k}_\perp)$, where

$$\mathcal{V}(\tilde{k}_\perp) = \frac{3g}{8\pi g_{\rm dd}} - \frac{1}{2} + \frac{15[2\tilde{k}_\perp^3 - 3\tilde{k}_\perp^2 - 3(1+\tilde{k}_\perp)^2\exp(-2\tilde{k}_\perp) + 3]}{8\tilde{k}_\perp^5}, \tag{1}$$

$\tilde{k}_\perp = k_\perp R_z$, and g is the contact interaction between the bosons. $\mathcal{V}(k_\perp)$ is repulsive for small momentum and can be attractive in the high-momentum limit depending on the contact interaction. Subsequently, we write the Hamiltonian of the dipolar bosons in the condensed phase, $H_b = \sum_{\vec{k}_\perp}\Omega_0(\vec{k}_\perp)\beta^\dagger_{\vec{k}_\perp}\beta_{\vec{k}_\perp}$, where $\beta^\dagger_{\vec{k}_\perp}$ and $\beta_{\vec{k}_\perp}$ are Bugoliubov operators. The excitation frequency $\Omega_0(\vec{k}_\perp)$ is given in the units of trap frequency,

$$\Omega_0^2(k_\perp\ell_0) = \frac{[k_\perp\ell_0]^4}{4} + g_{3\rm D}\frac{\ell_0}{R_z}\mathcal{V}\left(k_\perp\ell_0\frac{R_z}{\ell_0}\right)[k_\perp\ell_0]^2, \tag{2}$$

where $\ell_0 = \sqrt{\hbar/m_b\omega_b}$. We define a dimensionless dipolar interaction strength $g_{3\rm D} = 8\pi m_b g_{\rm dd} n_b \ell_0/5\hbar^2$ which will be used later, where ℓ_0 is the ground-state oscillator length. Also, the phonon propagator $D_0(i\omega_s,k_\perp)$ in this regime is given by

$$D_0(i\omega_s,k_\perp) = -\frac{\Omega_0(k_\perp)}{\omega_s^2 + \Omega_0^2(k_\perp)}, \tag{3}$$

where bosonic Matsubara frequency $\omega_s = 2s$, where s is an integer. By minimizing the mean-field energy of the Bose-Einstein condensate within the Thomas-Fermi regime, we find that

$$R_z/\ell_0 = \left(2.5g_{3\rm D}\left[1 + \frac{3}{16\pi g_{\rm dd}}\right]\right)^{1/3}.$$

For $\frac{3g}{4\pi g_{\rm dd}} > 1$, the excitation spectrum of the condensate, denoted by $\Omega(\vec{k}_\perp)$, can be divided into two parts: (i) $\sim k_\perp$, phonon spectrum for small momenta, and (ii) $\sim k_\perp^2$, free-particle-like spectrum for higher momenta [33]. For $\frac{3g}{4\pi g_{\rm dd}} < 1$ and $g_{3\rm D}$ greater than a critical value, $\Omega(\vec{k}_\perp)$ has a minimum at momentum $\tilde{k}_0$ [34], where $\tilde{k}_0$ is in intermediate momentum regime. Following Landau, the excitations around the minimum are called "rotons." With increasing $g_{3\rm D}$, the excitation energy at $\tilde{k}_0$ decreases and eventually vanishes for a critical particle density. When the particle density exceeds that critical value, the excitation energy becomes imaginary at finite momentum and the condensate becomes unstable. The use of Thomas-Fermi density profile is justified in this region as the chemical potential necessary to reach roton instability exceeds $\hbar\omega_z$ [34].

III. BOSON-FERMION INTERACTION AND DRESSED EXCITATION

In this section, first we disccuss the condensate-fermion interaction Hamiltonian and dynamical stability of the condensate. We find the the dressed propagator for the Bugoliubov quasiparticles in the presence of fermionic particle hole excitation within second-order perturbation theory. We then discuss the appearance of roton instability in the dressed excitation spectrum of the condensate.

Kinetic energy for the single-component fermions is characterized by the Hamiltonian $H_f = \sum_{\vec{k}_\perp}[\xi(\vec{k}_\perp) - \epsilon_F]c^\dagger_{\vec{k}_\perp}c_{\vec{k}_\perp}$, where $c^\dagger_{\vec{k}_\perp}$ and $c_{\vec{k}_\perp}$ are fermionic creation and destruction operators. $\xi(\vec{k}_\perp) = \vec{k}^2/2m_f - \epsilon_F$ is the dispersion energy of the fermions and ϵ_F is the Fermi energy. The density profile of fermions along the z direction is approximated by a normalized Gaussian with width $\ell_f = \sqrt{\hbar/m_f\omega_f}$. The fermions are interacting with the bosons via short-range contact interaction of strength $g_{\rm bf}$. After integrating over the z coordinate, the boson-fermion interaction Hamiltonian reads

$$H_{\rm bf} = \frac{3g_{\rm bf}\alpha}{4\sqrt{\pi}R_z}\sum_{\vec{k}_\perp,\vec{q}_\perp} c^\dagger_{\vec{k}_\perp}c_{\vec{k'}_\perp}b^\dagger_{\vec{q'}_\perp}b_{\vec{q}_\perp}, \tag{4}$$

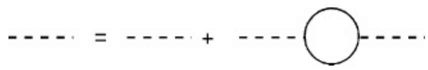

FIG. 1. Schematic diagram of phonon propagator including the polarizing effect of the fermions. The thick dashed line corresponds to the dressed phonon propagator $D(i\omega_s,k_\perp)$, while the thin dashed line corresponds to noninteracting phonon propagator $D_0(i\omega_s,k_\perp)$. The solid line corresponds to the free fermion propagator.

where $b_{\vec{q}_\perp}$ and $b^\dagger_{\vec{q}_\perp}$ are the bosonic creation and annihilation operators and $\alpha = \frac{\ell_f}{R_z}\exp(-\frac{R_z^2}{\ell_f^2}) - \frac{\sqrt{\pi}}{2}(\frac{\ell_f^2}{R_z^2} - 2)\mathrm{erf}(\frac{R_z}{\ell_f})$, with erf(...) being the error function. Next we concentrate our attention on the interaction between the fermions and the Bugoliubov quasiparticles. The fluctuations in fermionic density couple to the density fluctuations present in the Bose-Einstein condensate. Due to the momentum dependence of the bosonic excitations, the condensate-fermion interaction becomes a function of momentum. Including the fluctuations in the Bose-Einstein condensate in the x-y plane, the condensate-fermion interaction Hamiltonian can be written as

$$H_{\mathrm{bf}} = \frac{3g_{\mathrm{bf}}}{4\sqrt{\pi}R_z}\alpha \sum_{\vec{k}_\perp,\vec{q}_\perp} \gamma(\vec{k}_\perp) c^\dagger_{\vec{k}_\perp} c_{\vec{q}_\perp-\vec{k}_\perp}[b_{\vec{k}_\perp} + b^\dagger_{-\vec{k}_\perp}], \tag{5}$$

where the momentum-dependent coupling constant is given by $\gamma(\vec{k}_\perp) = \sqrt{2n_b\epsilon_b(\vec{k}_\perp)/\Omega_0(\vec{k}_\perp)}$. Due to the interaction between Bugoliubov quasiparticles and fermions, as shown in Fig. 1, the bosonic excitations are dressed by the fermions resulting in the dressing of the bare condensate excitation spectrum in Eq. (2). This can be derived within second-order perturbation theory as shown in Fig. 1. Subsequently, the new phonon propagator is given by

$$D(i\omega_s,k_\perp) = -\frac{\Omega_0(k_\perp)}{\omega_s^2 + \Omega^2(k_\perp)}, \tag{6}$$

where the dressed excitation spectrum $\Omega(k_\perp\ell_0)$ for the dressed Bugoliubov quasiparticles is expressed by

$$\Omega(\vec{k}_\perp) = \Omega_0(\vec{k}_\perp)\sqrt{1 - \frac{|\gamma(\vec{k}_\perp)|^2 N_0}{\Omega_0(k_\perp)} h(\omega,k_\perp)}, \tag{7}$$

where the two-dimensional Lindhard function

$$h(\omega,k_\perp) = 1 - |\omega|\frac{\theta(|\omega| - v_f k_\perp)}{\sqrt{\omega^2 - v_f^2 k_\perp^2}},$$

and ω is the transfer of energy. As we are interested in Cooper instability of the fermions which happens for momenta close to Fermi momentum, the transfer of energy is of the order of $\omega \ll \epsilon_F$. In this limit the Lindhard function $h(\omega,k_\perp) = 1$. For future use, we define an effective interaction strength between the bosons and the fermions,

$$\mathcal{G}_{\mathrm{bf}} = \frac{45 g_{\mathrm{bf}}^2 N_0}{128\pi g_{\mathrm{dd}}\ell_0}\alpha^2.$$

In order to determine dynamical stability of the uniform condensate, we study the properties of the dressed spectrum of Bugoliubov quasiparticles in the parameter regime of $\frac{3g}{4\pi g_{\mathrm{dd}}} > 1$, where the bare spectrum has no roton minimum. From Eq. (7), due to the attractive effect of Bose-Fermi interaction, we notice that roton minimum in the excitation spectrum $\Omega(\vec{k}_\perp)$ can develop for a certain critical interaction strength $g_{3\mathrm{D}}$ and G_{bf}. Consequently, the uniform condensate will become instable as the excitation spectrum becomes imaginary at a finite momentum. However, as long as the roton gap remains positive, the uniform state of the bosons will be stable or metastable [35]. In Fig. 2, we have plotted the dressed excitation spectrum for different values of Bose-Fermi interaction G_{bf}. With no boson-fermion interaction, as $\frac{3g}{4\pi g_{\mathrm{dd}}} > 1$, the excitation spectrum has the usual phonon regime for low momenta and free-particle regime for higher momenta. For a critical G_{bf}, that is, $G_{\mathrm{bf}} \approx 0.5$ in Fig. 2, in the region of intermediate momenta, the excitation spectrum has a roton-maxon character. With further increase of G_{bf}, the roton gap goes to zero and the excitation spectrum becomes imaginary at a finite momentum. Subsequently, the bosons undergo a phase transition to a state with periodic density modulation, which finally collapses. This periodic density wave state can be stabilized for repulsive contact interaction obeying $3g/8\pi g_{\mathrm{dd}} \approx \mathcal{G}_{\mathrm{bf}}\frac{\ell_0}{R_z}$ [35]. The appearance of a roton minimum in dressed excitation spectrum in this case is entirely due to the many-body effect of the fermions on Bugoliubov quasiparticles. Another point we like to stress is that the roton instability is always reached before the phonon instability pointing toward phase separation [19].

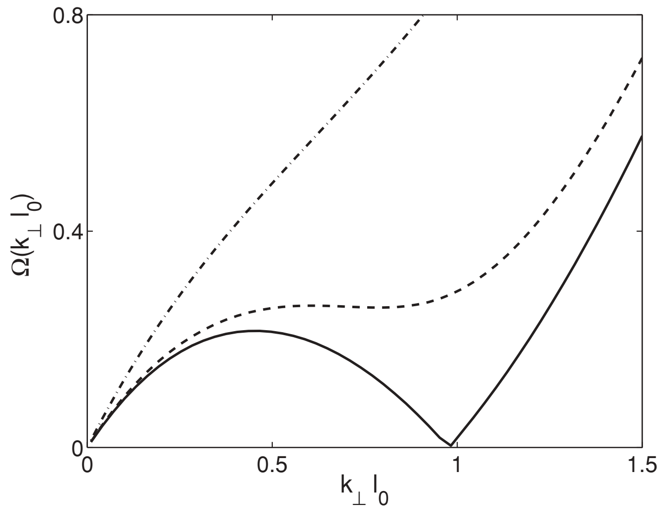

FIG. 2. The dressed excitation spectrum $\Omega(\vec{k}_\perp)$ (in units of $\hbar\omega_b$) as a function of $\vec{k}_\perp$ for various values of the Bose-Fermi interaction: $\mathcal{G}_{\mathrm{bf}} = 0$ (upper dash-dotted line), 0.51 (middle dashed line), and 0.57 (bottom solid line). The fixed parameters are $m_f = 53$, $\frac{3g}{4\pi g_{\mathrm{dd}}} = 0.6$, and $g_{3\mathrm{D}} = 2.5$.

IV. EFFECTIVE INTERACTION BETWEEN FERMIONS

In this section we find the interaction between the fermions mediated by the Bugoliubov quasiparticles in the limit of $T = 0$. We then obtain the interaction strength in a different angular momentum channel, which varies as a function of *dimensionality* parameter, defined as $\eta = \epsilon_F/\hbar\omega_f$.

Integrating out the bosonic degree of freedom in Eq. (5) and inclusion of the effect of dressed excitation spectrum result in

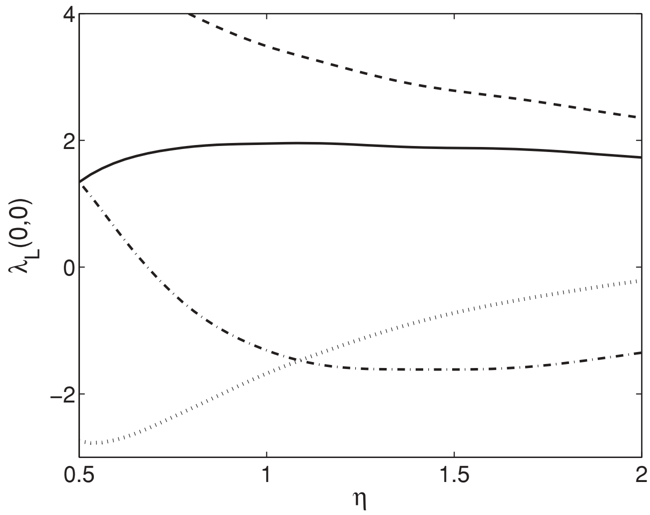

FIG. 3. Effective fermion-fermion interaction strength $\lambda_L(0,0)$ in the angular momentum channels $L=0$ (dashed line), $L=1$ (solid line), $L=3$ (dotted line), and $L=5$ (dash-dotted line) as functions of the fermion dimensionality parameter η. We fixed $m_f/m_b = 53/52$, $g_{3\mathrm{D}} = 4$, $3g/8\pi g_{\mathrm{dd}} = 0.6$, and $\mathcal{G}_{\mathrm{bf}} = 0.5$.

effective interaction between the fermions [36],

$$V_{\mathrm{ph}}(\vec{q}_\perp, i\omega_s) = \frac{9g_{\mathrm{bf}}^2\alpha^2}{16\pi R_z^2}\frac{n_b q_\perp^2/m_b}{\omega^2 - \Omega^2(\vec{q}_\perp)}, \tag{8}$$

where $q_\perp^2 = 2k_F^2(1-\cos\phi)$ is the momentum exchange between the interacting particles along the Fermi surface. At $T=0$, assuming momentum transfer occurs around the Fermi momentum k_F, we can expand Eq. (8) as $V_{\mathrm{ph}}(\vec{k}_\perp,0) = -\sum_{L=\ldots,-1,0,1,\ldots}\lambda_L(0,0)e^{iL\phi}$, and the dimensionless effective interaction between the fermions in angular momentum channel L is given by

$$\lambda_L(0,0) = \mathcal{G}_{\mathrm{bf}}\int_0^{2\pi}\frac{\exp[iL\phi]d\phi/2\pi}{\frac{\eta R_z^2}{g_{3\mathrm{D}}\ell_f^2}(1-\cos\phi) + \frac{R_z}{\ell_0}\mathcal{V}\left(\sqrt{\frac{R_z}{\ell_f}}\eta(1-\cos\phi)\right)}. \tag{9}$$

As we are considering single-component fermions, pairing will occur in the odd angular momentum channels.

Next we look into the variation of $\lambda_L(0,0)$ as a function of η. For concreteness, we assume a ^{52}Cr-^{53}Cr mixture. The interaction strengths from Eq. (9) in various angular momentum channels have been plotted in Fig. 3. We find that with changing dimensionality, the strengths in different angular momentum channels vary. Additionally, $|\lambda_1(0,0)| \sim |\lambda_3(0,0)| \sim |\lambda_5(0,0)|$, and, depending on the dimensionality, they can be positive or negative.

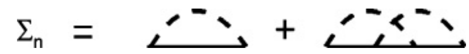

FIG. 4. Fermion self-energy in normal state including the first-order vertex correction. The solid line denotes the fermion propagator while the thick dashed line denotes the dressed phonon propagator of Eq. (6).

V. FERMIONIC SELF-ENERGY INCLUDING VERTEX CORRECTION

In this section, we consider the fermion self-energy in the normal state due to the interaction between the fermions and dressed Bugoliubov quasiparticles. In doing so, we explicitly take into account the momentum dependence as well as the retardation of the phonon propagator. More importantly, we also go beyond Migdal's adiabatic limit and take into account the effect of vertex correction. This kind of nonadiabatic correction is introduced to the electron-phonon system in metals in Refs. [37–39] in the limit of $T \to 0$. Our main result is that as temperature gets lower, the vertex-corrected mass renormalization function $Z(T)$ also gets smaller.

The unperturbed Green's function for the fermions is given by $G_0(\vec{k}_\perp, i\omega_n) = 1/[i\omega_n - \xi(\vec{k}_\perp)]$, where the Matsubara frequency $\omega_n = (2n+1)\pi T$, n being an integer. The normal self-energy $\Sigma_n(\vec{k}_\perp)$, including the first-order vertex correction, as shown in Fig. 4, is given by

$$\Sigma_n(\vec{k}_\perp, i\omega_n) = \Sigma_n^1(\vec{k}_\perp, i\omega_n) + \Sigma_n^v(\vec{k}_\perp, i\omega_n), \tag{10}$$

where $\Sigma_n^1(\vec{k}_\perp, i\omega_n)$ comes from the first diagram in Fig. 4 and $\Sigma_n^v(\vec{k}_\perp, i\omega_n)$ arises from the second diagram, which denotes the vertex correction. Also,

$$\Sigma_n^1(\vec{k}_\perp, i\omega_n) = -T\sum_{m,\vec{q}_\perp}|\gamma(\vec{k}_\perp - \vec{q}_\perp)|^2 \times D(\omega_m - \omega_n, \vec{k}_\perp - \vec{q}_\perp)G_0(i\omega_m, \vec{q}_\perp), \tag{11}$$

$$\begin{aligned}\Sigma_n^v(\vec{k}_\perp, i\omega_n) = T^2 &\sum_{m,l,\vec{q}_\perp,\vec{p}_\perp}|\gamma(\vec{k}_\perp - \vec{q}_\perp)|^2|\gamma(\vec{k}_\perp - \vec{p}_\perp)|^2 \\ &\times D(\omega_l - \omega_n, \vec{k}_\perp - \vec{p}_\perp)D(\omega_m - \omega_n, \vec{k}_\perp - \vec{q}_\perp) \\ &\times G_0(i\omega_m, \vec{q}_\perp)G_0(i\omega_l, \vec{p}_\perp)G_0 \\ &\times [i(\omega_l - \omega_n + \omega_m), \vec{p}_\perp - \vec{k}_\perp + \vec{q}_\perp],\end{aligned} \tag{12}$$

by taking the average over Fermi energy ($|\vec{k}_\perp| \approx |\vec{q}_\perp| \approx k_f$) and denoting $\xi(\vec{k}_\perp) = \hbar^2k_\perp^2/2m - \epsilon_F = x$, $\xi(\vec{p}_\perp) = \hbar^2k_\perp^2/2m - \epsilon_F = x'$, and $\xi(\vec{p}_\perp - \vec{k}_\perp\vec{q}_\perp) - \mu = x' + 2\epsilon_F\alpha$, where

$$\alpha = 1 - \cos(\phi') + \cos(\theta) - \cos(\gamma) \tag{13}$$

and the angles $(\vec{k}_\perp, \vec{q}_\perp) = \phi'$, $(\vec{k}_\perp, \vec{p}_\perp) = \theta$, and $\gamma = \phi' - \theta$. Using the Euler-Maclauren summation formula, we can transform the sum over l in Eq. (11) to integral as

$$\begin{aligned}P(x', m, T, \phi', \theta) &= -\sum_l D(\omega_l - \omega_n, \vec{k}_\perp - \vec{p}_\perp)G(i\omega_m, \vec{q}_\perp)G(i\omega_l, \vec{p}_\perp)G\big(i(\omega_l - \omega_n + \omega_m), \vec{p}_\perp - \vec{k}_\perp + \vec{q}_\perp\big) \\ &= \int_{-\infty}^{+\infty}\frac{d\omega}{2\pi}\frac{\Omega^2}{\omega^2 + \Omega^2}\frac{1}{i\omega - x' + i\pi T}\frac{1}{(\omega + 2m\pi T) - x' - \alpha + i\pi T}\end{aligned} \tag{14}$$

$$= \frac{i\Omega}{2(2m\pi T - i\alpha)}\left[\frac{\theta(x')}{\Omega + x' - i\pi T} - \frac{\theta(-x')}{\Omega - x' + i\pi T} - \frac{\theta(x'+\alpha)}{\Omega - 2im\pi T + x' - i\pi T + \alpha} + \frac{\theta(-x'-\alpha)}{\Omega + 2im\pi T - x' + i\pi T - \alpha}\right], \quad (15)$$

where $\theta(\ldots)$ is the step function. We can rewrite $\Sigma_n(i\omega_n)$ as

$$\Sigma_n(i\omega_n) = \chi(i\omega_n) + i\omega_n[1 - Z(i\omega_n)], \quad (16)$$

where $\chi(i\omega_n)$ is the real part of $\Sigma_n(i\omega_n)$ and $Z(i\omega_n)$ is known as the mass renormalization function. $\chi(\pi T)$ shifts the bare fermion dispersion energy $\xi(\vec{k}_\perp)$. As we are considering strong-coupling superfluidity, we only consider the term corresponding to $n = 0$ [40]. Then the mass renormalization functions $Z(\pi T)$ and $\chi(\pi T)$ in the conventional Eliashberg form is given by

$$Z(\pi T) = 1 + \lambda_Z(T), \quad (17)$$

$$\chi(\pi T) = \sum_m \mathrm{sgn}(\omega_m)\mathrm{Im}[P_v(m,T)], \quad (18)$$

with an effective coupling constant

$$\lambda_Z(T) = \lambda_0(0,0) - P_v^0(T), \quad (19)$$

and $P_v^0(T) = \sum_m \mathrm{sgn}(\omega_m)\mathrm{Re}[P_v^0(m,T)]$, where

$$\lambda_L(s,T) = -\int_0^{2\pi} |\gamma(\phi)|^2 D(\omega_s,\phi)(\cos L\phi)\, d\phi/2\pi,$$

$$P_v^L(m,T) = \int_{-\epsilon_F}^{\epsilon_F} dx' \int_{-\pi}^{\pi} \frac{d\phi'}{2\pi} \int_{-\pi}^{\pi} \frac{d\theta}{2\pi} |\gamma(\phi')|^2 |\gamma(\theta)|^2 \times P(x',m,T,\phi',\theta)(\cos L\theta), \quad (20)$$

and Re[f] and Im[f] denote the real and imaginary parts, respectively, of the function f. In Fig. 5 we plot $P_v^0(T)$ as a function of temperature for various values of dimensionality η. From the expression of $\lambda_L(s,T)$ in Eq. (20), we notice that $\lambda_L(0,0)$ is always positive, as shown in Fig. 3. $P_v^0(T)/\lambda_0(0,0)$ is the expansion parameter for the perturbative scheme. The correction $P_v^0(T)$ is always found to be positive, which reduces the coupling strength $\lambda_Z(T)$. With decreasing temperature, $P_v^0(T)/\lambda_0(0,0)$ increases before saturating. This saturation value increases with decreasing dimensionality, as seen in Fig. 5. For smaller $\eta, P_v^0(T)\lambda_0(0,0)$ becomes higher than one for lower temperature, invalidating any perturbative calculation in that low-temperature region.

Next we calculate the real part of the fermion self energy $\chi(\pi T)$. Figure 6 shows a such generic case for the same parameters as Fig. 5. We find that $\chi(T) \ll \lambda_0(0,0)$ even in the temperature region with high $P_v^0(T)$. Henceforth, we can neglect the effect of energy shift of the fermions due to the smallness of $\chi(T)$.

VI. SELF-ENERGY IN COOPER-PAIR CHANNEL AND TRANSITION TEMPERATURE

In this section we look at the fermionic self-energy in the Cooper-pair channel, $\Sigma_s(\vec{k}_\perp, i\omega_n)$ as represented diagramatically in Fig. 7, close to transition temperature T_c. Then we find transition temperature within strong-coupling limit considering the terms $n = 0, -1$ [40,41]. The main results of this section are: (i) Depending on the angular momentum channel, the vertex-corrected interaction strength can increase as a function of dimensionality and temperature. (ii) The

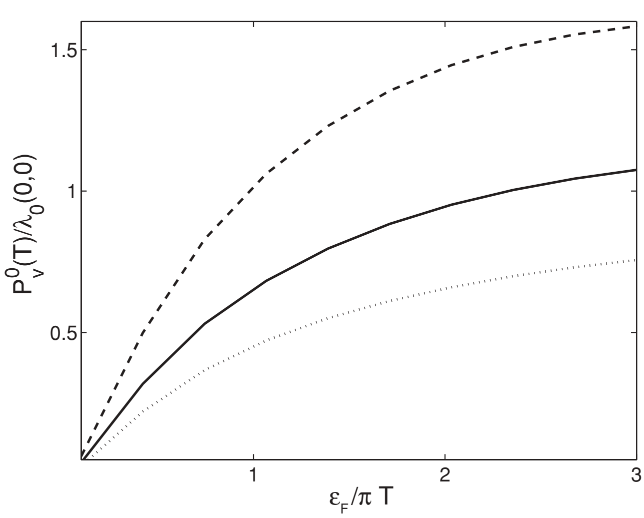

FIG. 5. Plot of the vertex correction in P_v^0 as a function of $\frac{\epsilon_F}{\pi T}$ for different values of the dimensionality parameter $\eta = 1.5$ (dotted line), $\eta = 1$ (solid line), and $\eta = 0.6$ (dashed line). We fixed $m_f/m_b = 53/52$, $\frac{3g}{4\pi g_{\rm dd}} = 0.6, \mathcal{G} = 0.5$, and $g_{3\rm D} = 3.8$.

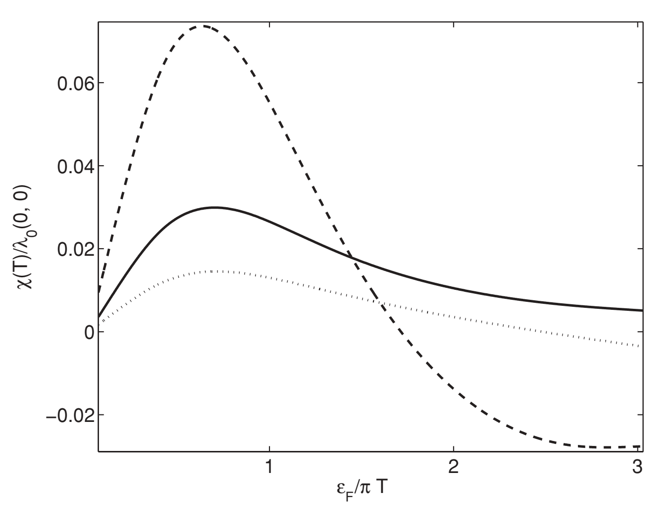

FIG. 6. $\chi(T)$ as a function of $\frac{\epsilon_F}{\pi T}$ for different values of the dimensionality parameter $\eta = 1.5$ (dotted line), $\eta = 1$ (solid line), and $\eta = 0.6$ (dashed line). We fixed $m_f/m_b = 53/52$, $\frac{3g}{4\pi g_{\rm dd}} = 0.6$, $\mathcal{G} = 0.5$, and $g_{3\rm D} = 3.8$.

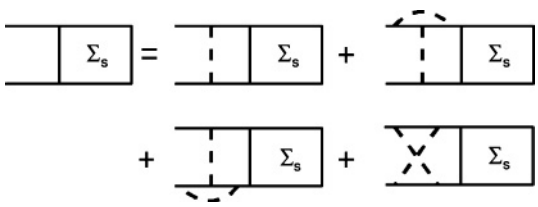

FIG. 7. Schematic diagram of fermion self-energy in the Cooper-pair channel including the first-order vertex correction. The solid line denotes the fermion propagator while the thick dashed line denotes the dressed phonon propagator of Eq. (6). The first diagram after the equals sign denotes the direct interaction, the second and third diagrams denote the first-order vertex corrections, and the fourth diagram denotes the cross-term.

solution of modified Eliashberg equation supports $T_c \sim 0.1\epsilon_F$ in the strong-coupling limit for p-, f-, and h-wave order parameters.

For $T > T_c$, the fermion self-energy in the Cooper-pair channel, $\Sigma_s(\vec{k}_\perp)$, is given by

$$\Sigma_s(\vec{k}_\perp,i\omega_n) = \Sigma_s^1(\vec{k}_\perp,i\omega_n) + \Sigma_s^v(\vec{k}_\perp,i\omega_n) + \Sigma_s^c(\vec{k}_\perp,i\omega_n), \tag{21}$$

where $\Sigma_s^1(\vec{k}_\perp,i\omega_n)$ comes from the first diagram after the equals sign in Fig. 7, the second and third diagrams give equal contribution and denoted by $\Sigma_s^v(\vec{k}_\perp,i\omega_n)$, while the last diagram, denoting cross interaction, is given by $\Sigma_s^c(\vec{k}_\perp,i\omega_n)$, and

$$\begin{aligned}\Sigma_s^1(\vec{k}_\perp,i\omega_n) &= -T\sum_{m,\vec{q}_\perp}|\gamma(\vec{k}_\perp-\vec{q}_\perp)|^2 D(\omega_m-\omega_n,\vec{k}_\perp-\vec{q}_\perp)\\ &\quad\times G(i\omega_m,\vec{q}_\perp)G(-i\omega_m,-\vec{q}_\perp)\Sigma_s(\vec{q}_\perp,i\omega_m),\end{aligned} \tag{22}$$

$$\begin{aligned}\Sigma_s^v(\vec{k}_\perp,i\omega_n) &= 2T^2\sum_{m,l,\vec{q}_\perp,\vec{p}_\perp}|\gamma(\vec{k}_\perp-\vec{q}_\perp)|^2|\gamma(\vec{k}_\perp-\vec{p}_\perp)|^2\\ &\quad\times D(\omega_m-\omega_n,\vec{k}_\perp-\vec{q}_\perp)D(\omega_n-\omega_l,\vec{k}_\perp-\vec{q}_\perp)\\ &\quad\times G(i\omega_l,\vec{p}_\perp)G\big(i(\omega_l-\omega_n+\omega_m),\vec{p}_\perp-\vec{k}_\perp+\vec{q}_\perp\big)\\ &\quad\times G(i\omega_m,\vec{q}_\perp)G(-i\omega_m,-\vec{q}_\perp)\Sigma_s(\vec{q}_\perp,i\omega_m),\end{aligned} \tag{23}$$

$$\begin{aligned}\Sigma_s^c(\vec{k}_\perp,i\omega_n) &= T^2\sum_{m,l,\vec{q}_\perp,\vec{p}_\perp}|\gamma(\vec{k}_\perp-\vec{p}_\perp)|^2|\gamma(\vec{q}_\perp-\vec{p}_\perp)|^2\\ &\quad\times D(\omega_n-\omega_l,\vec{k}_\perp-\vec{p}_\perp)D(\omega_m-\omega_l,\vec{q}_\perp-\vec{p}_\perp)\\ &\quad\times G(i\omega_l,\vec{p}_\perp)G\big(i(\omega_l-\omega_n-\omega_m),\vec{p}_\perp-\vec{k}_\perp-\vec{q}_\perp\big)\\ &\quad\times G(i\omega_m,\vec{q}_\perp)G(-i\omega_m,-\vec{q}_\perp)\Sigma_s(\vec{q}_\perp,i\omega_m).\end{aligned} \tag{24}$$

We take the average over Fermi energy($|\vec{k}_\perp| \approx |\vec{q}_\perp| \approx k_f$) and denote $\xi(\vec{p}_\perp - \vec{k}_\perp - \vec{q}_\perp) - \mu = x' + 2\epsilon_F\beta$, where

$$\beta = 1 + \cos(\phi') - \cos(\theta) - \cos(\gamma).$$

We define the superfluid order parameter in the usual way, $\Delta(i\omega_n) = \Sigma_s(i\omega_n)/Z(i\omega_n)$. Due to the single-component nature of the fermions in the mixture, the order parameter can be expanded in an odd partial wave $\Delta(i\omega_n,\phi) = \sum_{L=\dots,-1,1,\dots}\Delta_L(i\omega_n)\exp[iL\phi]$. In the strong coupling limit we are interested in the terms $n=0$ and $n=-1$. Assuming the order parameter to be an even function offrequency, $\Delta(\pi T) = \Delta(-\pi T)$, we get from Eqs. (21) and (22)

$$\Delta_L(\pi T)Z(\pi T) = \lambda_L^\Delta(0,T)\Delta_L(\pi T) + \lambda_L^\Delta(-1,T)\Delta_L(-\pi T), \tag{25}$$

where

$$\lambda_L^\Delta(m,T) = \lambda_L(m,T) - 2P_v^L(m,T) - P_c^L(m,T) \tag{26}$$

and $\lambda_L(m,T)$ originate from $\Sigma_s^1(i\omega_n)$, whereas $P_v^L(m,T)$ comes from the vertex-corrected self-energy $\Sigma_s^v(i\omega_n)$. $P_c(m,T)$ results from the contribution of the cross-term $\Sigma_s^c(i\omega_n)$,

$$\begin{aligned}P_c^L(m,T) &= 2T\,\mathrm{Im}\Bigg\{\sum_{l,\phi',\theta}(\cos L\theta)|\gamma(\theta)|^2|\gamma(\theta-\phi')|^2 D(l,\theta-\phi')\\ &\quad\times D(m-l,\theta)\left[\tan^{-1}\left(\frac{\epsilon_F}{(2l+1)\pi T}\right)-\tan^{-1}\right.\\ &\quad\times\left.\left(\frac{\epsilon_F}{i\beta+(2l-2m-1)\pi T}\right)\right]\frac{1}{\beta+2i(m+1)\pi T}\Bigg\}.\end{aligned} \tag{27}$$

Equation (25) is similar to the Eliashberg equation [40] in the strong coupling limit with additional vertex-corrected interaction strengths. Apart from the dependence on temperature, the effective interaction strength in the angular momentum channel $L,\lambda_L^\Delta(T)$, is also a function of dimensionality η and the boson-fermion mass ratio m_f/m_b. As noticed in Eq. (20), $P_v^L(0,T)$ is positive, thus reducing the effective interaction strength in the Cooper-pair channel. However, the correction arising from the cross term $P_c^L(m,T)$ can be negative or positive, as shown in Fig. 8. Also, the sign of $P_c^L(m,T)$ depends on the particular angular momentum channel under consideration. However, in general, for smaller $\eta, P_c^L(m,T)$ becomes positive, in turn reducing the interaction strength, $\lambda_L^\Delta(m,T)$, in the Cooper-pair channel. However, a higher value of η changes $P_c^L(m,T)$ to negative, which enhances $\lambda_L^\Delta(m,T)$. We also find out that with increasing fermionic mass, $P_c^L(m,T)$ becomes negative for lower values of η, thus enhancing the interaction strengths in the various angular momentum channel. The reason behind this is that $P_c^L(m,T)$ depends on the ratio between the position of the roton minimum k_0 and Fermi momentum $k_0/2k_f$. With high fermionic mass, k_f increases, resulting in a lower ratio $k_0/2k_f$. This in turn makes the cross term more negative. From this we infer that it is better to use fermions with higher mass to get a higher interaction strength $\lambda_L^\Delta(m,T)$.

Next we look into the dependence of $\lambda_L^\Delta(0,T)$ on dimensionality η. First we fix $\pi T = \epsilon_F$ and plot for various values of η in Fig. 9. We see that the magnitude of $\lambda_L^\Delta(\epsilon_F)$ in different angular momentum channels changes as η varies. Also, different angular momentum channels become dominant

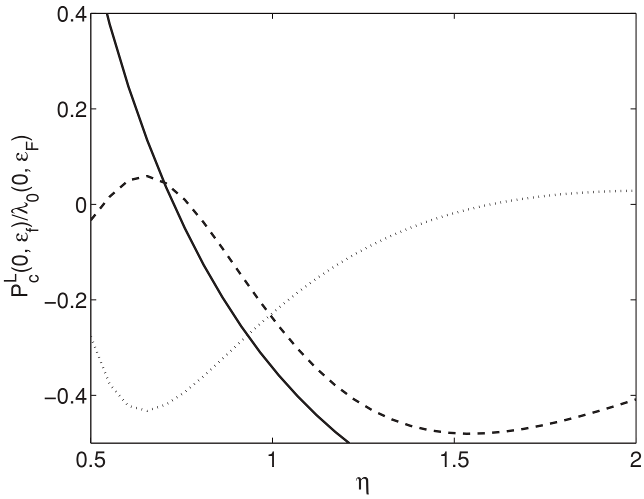

FIG. 8. Plot of cross-term interaction $P_c^L(0,\epsilon_F)$ as a function of η for $m_f/m_b = 53/52$, $\pi T = \epsilon_F$, $g_{3\mathrm{D}} = 4.0$, $\mathcal{G}_{\mathrm{bf}} = 0.5$, and $\frac{3g}{4\pi g_{\mathrm{dd}}} = 0.6$. From the left-hand side, the upper curve (solid line), the middle curve (dashed line), and the bottom curve (dotted line) correspond to p-, h-, and f-wave angular momentum channels, respectively.

depending on the dimensionality. This qualitatively resembles the situation in Sec. III, where without the vertex correction, we find that different interactions become dominant for different dimensionalities.

Next we find the transition temperature for fermionic superfluidity within a perturbative scheme as long as $T_c < T^*$, where T^* is the temperature for which the perturbative scheme becomes invalid. In the situation of more than one solution of Eq. (25), we have taken the transition temperature to be the one corresponding to the highest temperature. In the case of Eq. (25) having no solution for T_c, vertex-corrected strong coupling superfluidity is not possible and to find the transition temperature we need to consider the full Eliashberg equation [40] for all values of n. This regime is not considered

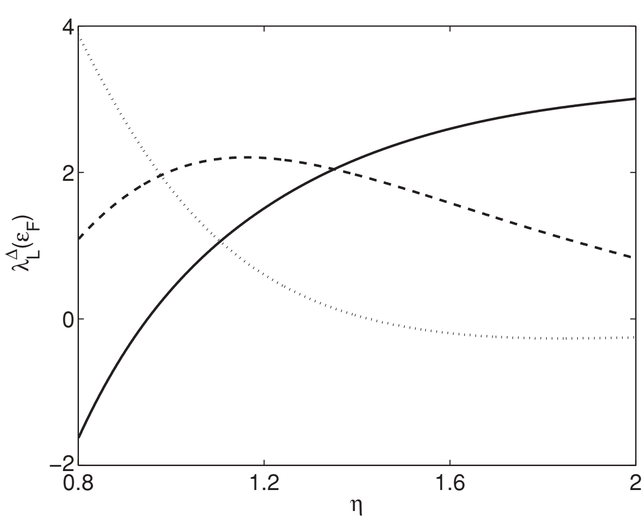

FIG. 9. Effective interaction $\lambda_L^\Delta(\pi T = \epsilon_F)$ as a function of η for $m_f/m_b = 53/52$, $\pi T = \epsilon_F$, $g_{3\mathrm{D}} = 4.0$, $\mathcal{G}_{\mathrm{bf}} = 0.5$, and $\frac{3g}{4\pi g_{\mathrm{dd}}} = 0.6$. From the left-hand side, the top curve (dotted line), the middle curve (dashed line), and the bottom curve (solid line) correspond to $\lambda_3^\Delta(T)$,$\lambda_5^\Delta(T)$, and $\lambda_1^\Delta(T)$, respectively.

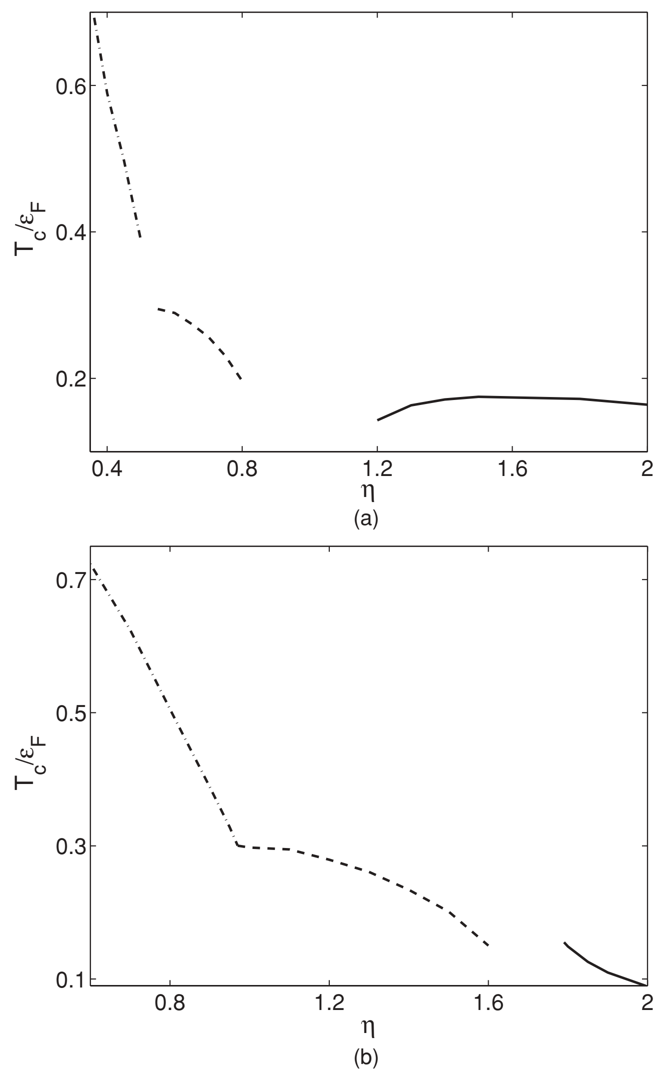

FIG. 10. Critical temperature T_c, in units of Fermi energy ϵ_F, as a function of η. The top curve (dash-dotted), the middle curve (dashed), and the bottom curve (solid) correspond to transition temperatures of p-wave, h-wave, and f-wave order parameters, respectively, with the following parameters: (a) $m_f/m_b = 1.7$, dipole strength $g_{3\mathrm{D}} = 2.5$; (b) $m_f/m_b = 53/52$, dipole strength $g_{3\mathrm{D}} = 4.0$.

in this article as we are only interested in the high-temperature limit of the transition temperature.

In Figs. 10(a) and 10(b) we plot the solution of Eqs. (17) and (25). In the case of obtaining multiple solutions for transition temperatures corresponding to different angular momentum channels, we considered the channel with maximum transition temperature to be the solution. In general, we find that with lowering dimensionality, the nature of the superfluidity changes from p to h to f wave. Also, we obtained transition temperature T_c on the order of $0.1\epsilon_F$ or more in each angular momentum channel. By comparing Figs. 10(a) and 10(b) we notice that, for higher fermion mass, we find that much lower value of η can be attainable without the perturbation becoming invalid than for a lower fermionic mass.

Thus, we find that, due to the rotonlike momentum dependence of the dressed excitation spectrum in the Bogoliubov propagator in Eq. (6), the sign and magnitude of vertex corrections depends strongly on the ratio $k_0/2k_f$. As we decrease η, for a fixed m_f,$k_0/2k_f$ increases; this in turn enhances the interaction strength in angular momentum channels $L = 3,5$, as shown in Fig. 9. This makes the vertex-corrected interaction strength in the Cooper-pair channel $\lambda_L^{\Delta}(T)$ stronger than $\lambda_Z^{\Delta}(T)$ in Eq. (17). In this case the solution of the conventional Eliashberg equation gives a transition temperature on the order of Fermi energy. In Refs. [41,42], using unbalanced Eliashberg equations, the authors find that transition temperature can be very high depending on the asymmetry of interactions in the normal channel and Cooper-pair channel. While deriving Eq. (25), we have neglected the effect of finite bandwidth of the system which is on the order of ϵ_F. When $T_c\ \epsilon_F$, as is the case for small η, the renormalization effect of the bandwidth will become prominent, resulting in a lower transition temperature, as discussed in Ref. [41].

VII. CHIRALITY AND NON-ABELIAN ANYONS

In this section we briefly discuss the properties of quasiparticle excitations inside a vortex for different internal symmetries of the order parameter. By solving a Bugoliubov–de Gennes equation in the limit of large distance from the core of the vortex, we show that the zero-energy solutions in the chiral p-, f-, h-wave states are bounded and non-Abelian in nature. By considering the superfluid gap equation at low temperature, the gap is maximum when the order parameter breaks time-reversal symmetry. From here on we assume that the order parameters are denoted by $\Delta_L = \Delta_0(\vec{r})[\frac{k}{k_f}]^L e^{iL\theta}$, where $k_x = k\cos\theta$, $k_y = k\sin\theta$, and $\Delta_0(\vec{r})$ is the center-of-mass amplitude of the Cooper pairs, with $\vec{r}$ being the center-of-mass coordinate of the pair. For a vortex state, $\Delta_0(\vec{r})$ can be approximated as: (i) $\Delta_0(\vec{r}) = 0$, $r < \xi$, and (ii) $\Delta_0(\vec{r}) = \Delta_0 \exp(i\phi)$, $r \geqslant \xi$, where $r = \sqrt{x^2+y^2}$ and $\tan\phi = y/x$. ξ is the size of the core of the vortex. The vortex state of the p-wave superfluids always has a zero-energy bound quasiparticle state [7,43–45]. Now we discuss the asymptotic solutions for the zero-energy bound state for f- and h-wave order parameters. The quasiparticle states in a single vortex can be found in the limit of large distance from the vortex core by solving the Bugoliubov–de Gennes equation,

$$\begin{aligned} &H_0 u_L + (-i)^L \frac{\Delta_0}{k_f^L} e^{i\phi/2}\left[e^{-i\phi}\left(\frac{\partial}{\partial r} - \frac{i}{r}\frac{\partial}{\partial\phi}\right)\right]^L e^{i\phi/2} v_L \\ &\quad = E u_L, \\ &-H_0 v_L + (i)^L \frac{\Delta_0}{k_f^L} e^{-i\phi/2}\left[e^{i\phi}\left(\frac{\partial}{\partial r} + \frac{i}{r}\frac{\partial}{\partial\phi}\right)\right]^L e^{-i\phi/2} u_L \\ &\quad = E v_L, \end{aligned} \tag{28}$$

where E is the energy of the quasiparticles with amplitudes u_L,v_L. We particularly look for zero-energy solutions with bounded u_L,v_L and the property $u_L = v_L^*$ [43]. For $r \to \infty$, we can neglect the terms scaled as r^{-1} in Eq. (28). Then the solution of Eq. (28) with different orbital symmetries reads

$$\begin{bmatrix} u_1 \\ u_3 \\ u_5 \end{bmatrix} \sim \begin{bmatrix} \exp\left(-\frac{m_f \Delta_0}{k_f} r\right) \\ \exp\left(-\frac{k_f^3}{6m_f\Delta_0} r\right) e^{2i\phi} \\ \exp\left(-\left[\frac{k_f^5}{2m_f\Delta_0}\right]^{1/3} r\right) e^{4i\phi} \end{bmatrix}. \tag{29}$$

The zero-energy solution for each odd-wave parameter corresponds to a different angular momentum channel of the quasiparticles inside a vortex core. These results can also be carried out by applying the "index theorem" [46]. For temperature smaller than the energy gap Δ_0^2/ϵ_F, only the zero-energy mode is occupied. The quasiparticle operator in that situation is written as $\gamma_L = \int d^2r[u_L(r)c^\dagger(r) + v_L(r)c(r)]$, which acts as a Majorana fermion [7,15,43]. γ_L obeys non-Abelian statistics and can be used for quantum computing [16]. In order to perform quantum computational tasks, the existence of several well-separated vortices is necessary. We can assume in the weak coupling limit $\Delta_0 = \beta\epsilon_F$, where β is a constant usually less than one. Then substituting Δ_0 in Eq. (29), we get $u_1 \propto \exp(-\beta k_f r/2)$, $u_3 \propto \exp(-k_f r/3\beta)$, and $u_5 \propto \exp(-k_f r/\beta^{1/3})$. For $r \gg \xi$, for smaller β,u_5 has a smaller tail than u_3 and u_1. Thus nonoverlapped states can be achieved more easily in superfluids in $L = 5$ and $L = 3$ channels than in a p-wave channel.

VIII. CONCLUSION

Summarizing, we studied boson-induced superfluidity of fermions in a mixture of dipolar bosons and single-component fermions. A system is proposed where a conventional pairing mechanism gives rise to different exotic internal structures of the Cooper pairs with strong interactions in respective angular momentum channels. We find that vertex corrections play an important role in superfluidity in this mixture and results in high values of transition temperatures. We like to stress that the high transition temperatures are a result of the inclusion of vertex corrections and cross interactions within the Cooper-pair channel. Importantly, we find that by decreasing η, we can generate exotic superfluids with p-, f-, and h-wave internal structures. Excitations in these types of superfluids breaks time-reversal symmetry and supports quasiparticles with non-Abelian statistics.

ACKNOWLEDGMENTS

This work is financially supported by the Spanish MEC QOIT (Consolider Ingenio 2010) projects, TOQATA (FIS2008-00784), MEC/ESF Project FERMIX (FIS2007-29996-E), EU IP Grant AQUTE, ERC advanced Grant QUAGATUA, and the Humboldt Foundation.

[1] M. W. Zwierlein *et al.*, Science **311**, 492 (2006).
[2] G. Barton and M. A. Moore, J. Phys. C **8**, 970 (1975).
[3] N. D. Mermin, Phys. Rev. B **13**, 112 (1976).
[4] M. Sigrist and K. Ueda, Rev. Mod. Phys. **63**, 239 (1991).
[5] Y. Maeno, T. M. Rice, and M. Sigrist, Phys. Today **54**, 42 (2001).

[6] R. L. Willett *et al.*, Phys. Rev. Lett. **59**, 1776 (1987).
[7] C. Nayak, S. H. Simon, A. Stern, M. Freedman, and S. Das Sarma, Rev. Mod. Phys. **80**, 1083 (2008).
[8] N. Read, Phys. Rev. B **79**, 045308 (2009).
[9] F. Wilczek, Phys. Rev. Lett. **48**, 1144 (1982).
[10] F. Wilczek, Phys. Rev. Lett. **49**, 957 (1982).
[11] F. Wilczek, *Fractional Statistics and Anyon Superconductivity* (World Scientific, Singapore, 1990).
[12] A. Y. Kitaev, Ann. Phys. **303**, 2 (2003).
[13] D. Marinaro and O. Sushkov, Phys. Rev. B **58**, 14934 (1998).
[14] D. Vollhardt and P. Woelfle, *The Superfluid Phases of 3He* (Taylor and Francis, Abingdon, UK, 1990).
[15] D. A. Ivanov, Phys. Rev. Lett. **86**, 268 (2001).
[16] S. Tewari, S. Das Sarma, C. Nayak, C. Zhang, and P. Zoller, Phys. Rev. Lett. **98**, 010506 (2007).
[17] J. Levinsen, N. R. Cooper, and V. Gurarie, Phys. Rev. A **78**, 063616 (2008).
[18] N. R. Cooper and G. V. Shlyapnikov, e-print arXiv:0907.3080.
[19] D. V. Efremov and L. Viverit, Phys. Rev. B **65**, 134519 (2002).
[20] J. Mur-Petit, A. Polls, M. Baldo, and H.-J. Schulze, Phys. Rev. A **69**, 023606 (2004).
[21] K. Yang, Phys. Rev. B **77**, 085115 (2008).
[22] K. Suzuki, T. Miyakawa, and T. Suzuki, Phys. Rev. A **77**, 043629 (2008).
[23] T. Enss and W. Zwerger, Eur. Phys. J. B **68**, 383 (2009).
[24] A. Bulgac and S. Yoon, Phys. Rev. A **79**, 053625 (2009).
[25] E. P. Bashkin and A. E. Meyerovich, Adv. Phys. **30**, 1 (1981).
[26] E. Ostgaard and E. P. Bashkin, Physica B **178**, 134 (1992).
[27] M. A. Baranov, A. V. Chubukov, and M. Yu. Kagan, Int. J. Mod. Phys. B **6**, 2471 (1992).
[28] D. V. Efremov, M. S. Mar'enko, M. A. Baranov, and M. Yu. Kagan, JETP **90**, 861 (2000).
[29] M. Yu. Kagan, Sov. Phys. Usp. **164**, 77 (1994).
[30] T. Lahaye *et al.*, Nature (London) **448**, 672 (2007).
[31] T. Koch *et al.*, Nat. Phys. **4**, 218 (2008).
[32] S. Ospelkaus, K. K. Ni, M. H. G. de Miranda, B. Neyenhuis, D. Wang, S. Kotochigova, P. S. Julienne, D. S. Jin, and J. Ye, e-print arXiv:0811.4618.
[33] L. Pitaevskii and S. Stringari, *Bose-Einstein Condensation* (Claredon Press, Oxford, UK, 2003).
[34] L. Santos, G. V. Shlyapnikov, and M. Lewenstein, Phys. Rev. Lett. **90**, 250403 (2003).
[35] O. Dutta, R. Kanamoto, and P. Meystre, Phys. Rev. A **78**, 043608 (2008).
[36] D.-W. Wang, Phys. Rev. Lett. **96**, 140404 (2006).
[37] C. Grimaldi, L. Pietronero, and S. Strassler, Phys. Rev. Lett. **75**, 1158 (1995).
[38] L. Pietronero, S. Strassler, and C. Grimaldi, Phys. Rev. B **52**, 10516 (1995).
[39] C. Grimaldi, L. Pietronero, and S. Strassler, Phys. Rev. B **52**, 10530 (1995).
[40] G. D. Mahan, *Many-Particle Physics*, 3rd ed. (Kluwer Academic/Plenum, New York, 2000).
[41] E. Cappelluti and G. A. Ummarino, Phys. Rev. B **76**, 104522 (2007).
[42] J. P. Carbotte, Rev. Mod. Phys. **62**, 1027 (1990).
[43] V. Gurarie and L. Radzihovsky, Phys. Rev. B **75**, 212509 (2007).
[44] G. E. Volovik, *The Universe in a Helium Droplet* (Clarendon Press, Oxford, UK, 2003).
[45] M. Yu. Kagan and D. V. Efremov, J. Low Temp. Phys. **158**, 749 (2010).
[46] S. Tewari, S. Das Sarma, and D.-H. Lee, Phys. Rev. Lett. **99**, 037001 (2007).